Communication-less Model Based Distributed Control for DC Microgrids

Ruihao Song, Branislav Hredzak, and Toan Phung
University of New South Wales, Sydney, Australia
Email: Ruihao.song@student.unsw.edu.au; {b.hredzak; toan.phung}@unsw.edu.au

***Abstract*—With the penetration of renewable energy, the electrical grid tends to be more flexible and distributed. Microgrid is a promising solution to deal with the rising challenges in distributed generation. Droop control is often adopted to handle power sharing for distributed generation control in microgrids, however it cannot guarantee required sharing accuracy and power quality to critical loads without using communication links. This paper proposes a method to achieve accurate current sharing without communication. One distributed generation (DG) is selected as a leader while the others are considered followers with a complete model of the leader. With the proposed method, the current can be shared with a desired ratio while the power quality remains unaffected.**

***Index Terms*—distributed generation, power sharing control, power quality restoration, DC microgrid**

NOMENCLATURE

K_{pv}	Voltage controller proportional gain
K_{iv}	Voltage controller integral gain
K_{pc}	Current controller proportional gain
K_{ic}	Current controller integral gain
K_{ps}	Secondary controller proportional gain
K_{is}	Secondary controller integral gain
k_{Fi}	Following ratio
φ	Voltage controller auxiliary state
γ	Current controller auxiliary state
i_r	Output filter inductor current
v_o	Output filter capacitor voltage
i_g	Output current to public load
v_i	Inverter output voltage
R_f	Filter inductor resistance
L_f	Filter inductor inductance
C_f	Filter capacitor capacitance
R_{Line}	Transmission line resistance
L_{Line}	Transmission line inductance
V_o^*	DC microgrid nominal voltage
v_b	Common coupling point (PCC) voltage
R_{Local}	Local load resistance

Manuscript received March 19, 2018; revised June 25, 2018; accepted July 30, 2018.

Corresponding author: Ruihao Song (email: Ruihao.song@student.unsw.edu.au)

" $\hat{x}$ " denotes estimated x, " $\tilde{x}$ " denotes estimation error of x, subscript "L" denotes leader system, subscript " Fi " denotes the i^{th} follower system, and superscript "*" denotes reference value.

I. INTRODUCTION

In modern power systems, the role of renewable generation becomes more and more important. New power electronic equipment will dominate the electrical grid in the next decades and in the meantime the electrical grids tend to be more distributed, intelligent, and flexible [1]-[3]. The concept of microgrid (MG) has been identified as an effective method for integration of future energy systems [4], [5]. However, all merits of future grids are based on one significant condition: proper control strategy must be adopted, otherwise the circulating currents flowing between the generation units may lead to instability of the microgrids.

Many renewable energy sources generate DC power, and with the increasing penetration of DC loads, such as digital devices, there is a growing interest in DC microgrids [6], [7]. Development of semiconductor based power conversion devices offers the possibility of flexible voltage/current transformation, and thus brings DC power into applications such as data centers, space exploration, offshore windfarms, electrical networks on ships, electrical vehicles, and HVDC transmission systems [8]–[15].

To make the microgrid operate normally, the current sharing accuracy and voltage regulation must be ensured at all time. Droop control is a commonly accepted method which allows smart grid operation without communication network. However, due to the line impedance differences between the generation units, the current sharing can have a significant error, and because of the nature of the droop control, the power quality is slightly degraded. It is noteworthy that the droop control suffers from the trade-off between the voltage regulation and current sharing accuracy. In [16] and [17], full models of the droop control system for AC and DC microgrid were derived, respectively. A centralized, higher level controller can be added to restore the power quality and eliminate the current sharing error as proposed in [18]. However, the centralized control structure is not flexible in terms of plug-and-play functionality, and when a link fails, a system level instability can occur [19]. A decentralized per-unit current sharing method was proposed in [20], using a

doi: 10.18178/ijeetc.8.3.139-145

low-bandwidth communication to compensate the drawbacks. In [21], a method to achieve current sharing by using the averaged voltage and current values was introduced. Unfortunately, this method only works for a double-unit system and extension to a multi-unit system is hard to achieve.

Recently, a more advanced method, considering each DG as an agent and thus requiring unit-to-unit communication rather than the traditional centralized structure, has been proposed in [22]-[26]. All agents try to minimize the error between their neighbors, and therefore the main control objective can be achieved by controlling the agent which is working as a "leader". It has been proven to be a more robust and efficient way to control a small-scale network. In recent literatures, multi-agent control method has become a main stream for microgrid control problems. Various algorithms and modelling methods were introduced to cover all possible conditions. In [27], a decentralized secondary control was designed to adapt to different types of communication network. Besides the communication topology, the inevitable noise in the transmission is also a critical issue which can potentially degrade the system performance. In [28], the effect of communication links noise on the synchronization process was studied in detail. The application of advanced nonlinear algorithms such as sliding-mode control for more robust control performance was introduced in [29].

In this paper, a method for reducing the current sharing error is proposed. The key idea is to make one unit a leader of the group and all followers have a mathematical model to simulate a virtual version of the leader system. Thus, the leader current is estimated locally, and the follower units follow the estimation results. The structure is similar to a master-slave configuration, but without a communication link. Therefore, the proposed system is relatively more reliable and robust. The major challenge of the proposed system is that all followers need to estimate the bus voltage of the leader unit to provide the input for the local model. The estimation can be inaccurate when the network line impedances are significant. A sensitivity analysis is performed to examine how much the current sharing is degraded with respect to the inaccurate estimation. Local secondary PI controller is introduced to force the follower systems to follow the estimated leader current references. A guide to design the controller gain is provided based on eigenvalue analysis of a small-signal model of one follower system. Finally, simulation in MATLAB/SIMULINK verifies performance of the proposed method.

II. System Modelling

This section introduces a small-signal model of the proposed system. The microgrid system consists of one leader and multiple followers, Fig. 1. The leader system has a single layer voltage and current control system, while the followers have a double layer hierarchical control structure. The primary layers of both the leader system and the follower systems are identical.

The key idea of the proposed method is in a localized secondary control layer without any communication. The secondary layer in the follower units follows the leader current, which is estimated using a virtual model of the leader system. The estimated current can be adjusted so that the followers converge to any ratio of the leader's current.

A. Leader System

Unlike traditional networks with many synchronous generators, microgrids are low inertia systems. In traditional networks the dynamics are usually dominated by the generators, while in the microgrid they are more dependent on the filters and network.

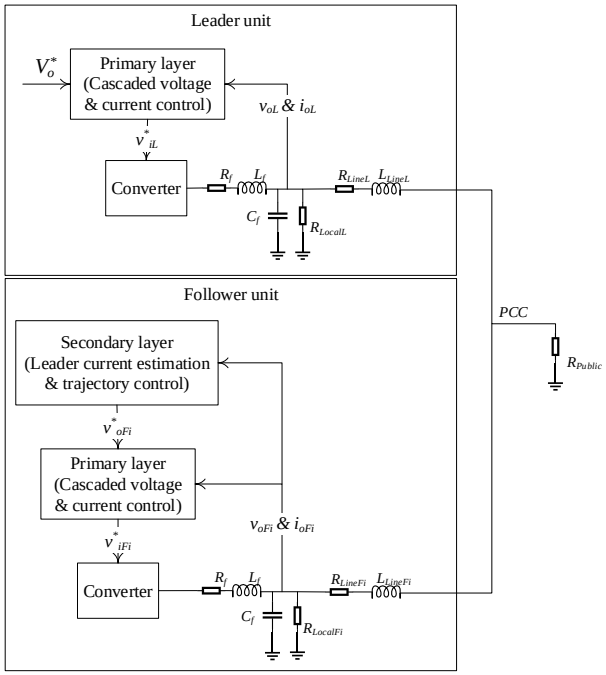

Fig. 1. Overview block diagram.

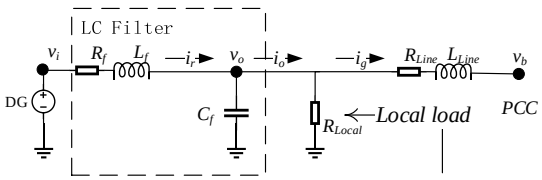

Fig. 2. Detail of connection from DG to PCC.

Due to the power electronic devices switching, the output of the converter contains harmonics which can affect the system's performance. To filter the noise and harmonics, a standard LC filter is used, Fig. 2. When the local load and line impedance are not negligible, the state equations of the leader system are,

$$\frac{di_{rL}}{dt} = -\frac{R_f}{L_f} i_{rL} + \frac{1}{L_f} v_{iL} - \frac{1}{L_f} v_{oL} \tag{1}$$

$$\frac{dv_{oL}}{dt} = \frac{1}{C_f} i_{rL} - \frac{1}{C_f} i_{gL} - \frac{1}{C_f R_{LocalL}} v_{oL} \tag{2}$$

$$\frac{di_{gL}}{dt} = -\frac{R_{LineL}}{L_{LineL}} i_{gL} + \frac{1}{L_{LineL}} v_{oL} - \frac{1}{L_{LineL}} v_{bL} \tag{3}$$

The above equations can be linearized with the inputs being the converter output and PCC voltages. A small-signal state space model combining the LC filter, local load and line impedance is,

$$\begin{bmatrix}\Delta\dot{i}_{rL}\\ \Delta\dot{v}_{oL}\\ \Delta\dot{i}_{gL}\end{bmatrix}=A_{oL}\begin{bmatrix}\Delta i_{rL}\\ \Delta v_{oL}\\ \Delta i_{gL}\end{bmatrix}+B_{oL1}\Delta v_{iL}^{*}+B_{oL2}\Delta v_{bL}$$

$$A_{oL}=\begin{bmatrix}-\frac{R_f}{L_f} & -\frac{1}{L_f} & 0\\ \frac{1}{C_f} & -\frac{1}{C_f R_{LocalL}} & -\frac{1}{C_f}\\ 0 & \frac{1}{L_{LineL}} & -\frac{R_{LineL}}{L_{LineL}}\end{bmatrix} \quad (4)$$

$$B_{oL1}=\begin{bmatrix}\frac{1}{L_f} & 0 & 0\end{bmatrix}^{T},\ B_{oL2}=\begin{bmatrix}0 & 0 & -\frac{1}{L_{LineL}}\end{bmatrix}^{T}$$

The leader has only the primary control layer. The purpose of leader is to provide a reference for the followers and thus its voltage reference does not vary with time. Cascaded voltage and current control is achieved using PI controllers. The equations of this primary control layer can be written as,

$$\frac{d\varphi_L}{dt}=v_{oL}^{*}-v_{oL} \quad (5)$$

$$i_{oL}^{*}=K_{pv}(v_{oL}^{*}-v_{oL})+K_{iv}\varphi_L \quad (6)$$

$$\frac{d\gamma_L}{dt}=i_{oL}^{*}-i_{oL}=i_{oL}^{*}-i_{gL}-\frac{1}{R_{LocalL}}v_{oL} \quad (7)$$

$$v_{iL}^{*}=K_{pc}\left(i_{oL}^{*}-i_{gL}-\frac{1}{R_{LocalL}}v_{oL}\right)+K_{ic}\gamma_L \quad (8)$$

By linearizing the equations above, a small-signal model of the cascaded voltage and current controller can be written in the state-space form as in (9). The inputs are the reference, measured voltage and currents. Two auxiliary states are introduced to assist with the dynamics modelling. The output is the required output voltage for the converters.

$$\begin{bmatrix}\Delta\dot{\varphi}_L\\ \Delta\dot{\gamma}_L\end{bmatrix}=A_{vc}\begin{bmatrix}\Delta\varphi_L\\ \Delta\gamma_L\end{bmatrix}+B_{vc1}\begin{bmatrix}\Delta i_{rL}\\ \Delta v_{oL}\\ \Delta i_{gL}\end{bmatrix}+B_{vc2}\Delta v_{oL}^{*}$$

$$\begin{bmatrix}\Delta v_{iL}^{*}\end{bmatrix}=C_{vc}\begin{bmatrix}\Delta\varphi_L\\ \Delta\gamma_L\end{bmatrix}+D_{vc1}\begin{bmatrix}\Delta i_{rL}\\ \Delta v_{oL}\\ \Delta i_{gL}\end{bmatrix}+D_{vc2}\Delta v_{oL}^{*}$$

$$A_{vc}=\begin{bmatrix}0 & 0\\ K_{iv} & 0\end{bmatrix}\quad B_{vc1}=\begin{bmatrix}0 & -1 & 0\\ 0 & -K_{pv}-\frac{1}{R_{LocalL}} & -1\end{bmatrix}$$

$$B_{vc2}=\begin{bmatrix}1 & K_{pv}\end{bmatrix}^{T},\quad C_{vc}=\begin{bmatrix}K_{pc}K_{iv} & K_{ic}\end{bmatrix}$$

$$D_{vc1}=\begin{bmatrix}0 & -K_{pc}K_{pv}-\frac{K_{pc}}{R_{LocalL}} & -K_{pc}\end{bmatrix}$$

$$D_{vc2}=K_{pc}K_{pv} \quad (9)$$

The resulting closed-loop state-space model is shown in (10). Because the leader unit is under fixed voltage control, the first input Δv_{ol}^{*}, which is the voltage reference disturbance to the inner cascaded voltage and current loop, is always zero, and thus the corresponding term can be ignored.

$$\begin{bmatrix}\Delta\dot{\varphi}_L\\ \Delta\dot{\gamma}_L\\ \Delta\dot{i}_{rL}\\ \Delta\dot{v}_{oL}\\ \Delta\dot{i}_{gL}\end{bmatrix}=A_L\begin{bmatrix}\Delta\varphi_L\\ \Delta\gamma_L\\ \Delta i_{rL}\\ \Delta v_{oL}\\ \Delta i_{gL}\end{bmatrix}+B_{L1}\Delta v_{oL}^{*}+B_{L2}\Delta v_{bL}+B_{L1}V_o^{*}$$

$$A_L=\begin{pmatrix}A_{vc} & B_{vc1}\\ B_{oL1}C_{vc} & A_{oL}+B_{oL1}D_{vc1}\end{pmatrix} \quad (10)$$

$$B_{L1}=\begin{pmatrix}B_{vc2}\\ B_{oL1}D_{vc2}\end{pmatrix}\quad B_{L2}=\begin{pmatrix}0_{2*1}\\ B_{oL2}\end{pmatrix}$$

B. Follower System

Follower systems have the same structure as the leader, but the local load and line impedance can be different. Therefore, for the primary layer, the dynamics can be obtained easily by swapping the electrical parameters in (10),

$$\begin{bmatrix}\Delta\dot{\varphi}_{Fi}\\ \Delta\dot{\gamma}_{Fi}\\ \Delta\dot{i}_{rFi}\\ \Delta\dot{v}_{oFi}\\ \Delta\dot{i}_{gFi}\end{bmatrix}=A_{Fi}\begin{bmatrix}\Delta\varphi_{Fi}\\ \Delta\gamma_{Fi}\\ \Delta i_{rFi}\\ \Delta v_{oFi}\\ \Delta i_{gFi}\end{bmatrix}+B_{Fi1}\Delta v_{oFi}^{*}+B_{Fi2}\Delta v_{bFi}+B_{Fi1}V_o^{*} \quad (11)$$

where

$$A_{Fi}=\begin{pmatrix}A_{vc} & B_{vc1}\\ B_{oFi1}C_{vc} & A_{oFi}+B_{oFi1}D_{vc1}\end{pmatrix}$$

$$B_{Fi1}=\begin{pmatrix}B_{vc2}\\ B_{oFi1}D_{vc2}\end{pmatrix}\quad B_{Fi2}=\begin{pmatrix}0_{2*1}\\ B_{oFi2}\end{pmatrix}$$

$$A_{oFi}=\begin{bmatrix}-\frac{R_f}{L_f} & -\frac{1}{L_f} & 0\\ \frac{1}{C_f} & -\frac{1}{C_f R_{localFi}} & -\frac{1}{C_f}\\ 0 & \frac{1}{L_{LineFi}} & -\frac{R_{LineFi}}{L_{LineFi}}\end{bmatrix}$$

$$B_{oFi1}=\begin{bmatrix}\frac{1}{L_f} & 0 & 0\end{bmatrix}^{T},\ B_{oFi2}=\begin{bmatrix}0 & 0 & -\frac{1}{L_{LineFi}}\end{bmatrix}^{T}$$

However, compared with the leader system, the proposed follower system has an additional local secondary control layer to adjust the inner primary control reference to achieve the current sharing. An illustration diagram is shown in Fig. 3. The local secondary control layer dynamics can be linearized into a small signal model as:

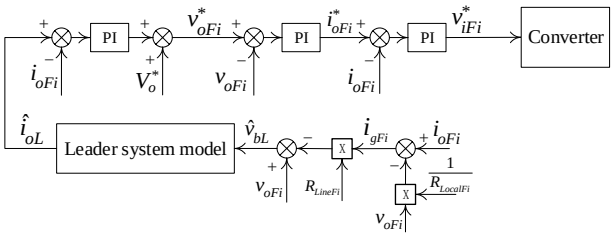

Fig. 3. Block diagram of follower system.

$$\Delta\dot{\varepsilon}_{Fi} = B_{s1}\Delta\hat{i}_{oL} + B_{s2}\begin{bmatrix}\Delta\varphi_{Fi}\\ \Delta\gamma_{Fi}\\ \Delta i_{rFi}\\ \Delta v_{oFi}\\ \Delta i_{gFi}\end{bmatrix}$$

$$\Delta v^{*}_{oFi} = C_s\Delta\varepsilon_{Fi} + D_{s1}\Delta\hat{i}_{oL} + D_{s2}\begin{bmatrix}\Delta\varphi_{Fi}\\ \Delta\gamma_{Fi}\\ \Delta i_{rFi}\\ \Delta v_{oFi}\\ \Delta i_{gFi}\end{bmatrix}$$

$$B_{s1} = k_{Fi} \quad B_{s2} = \begin{bmatrix}0 & 0 & 0 & -\dfrac{1}{R_{LocalFi}} & -1\end{bmatrix} \quad (12)$$

$$C_s = K_{is} \quad D_{s1} = K_{ps}$$

$$D_{s2} = \begin{bmatrix}0 & 0 & 0 & -\dfrac{K_{ps}}{R_{LocalFi}} & -K_{ps}\end{bmatrix}$$

The required reference for the local secondary control is generated by the mathematical model of the leader system from the previous analysis.

$$\begin{bmatrix}\Delta\dot{\hat{\varphi}}_L\\ \Delta\dot{\hat{\gamma}}_L\\ \Delta\dot{\hat{i}}_{rL}\\ \Delta\dot{\hat{v}}_{oL}\\ \Delta\dot{\hat{i}}_{gL}\end{bmatrix} = A_L\begin{bmatrix}\Delta\hat{\varphi}_L\\ \Delta\hat{\gamma}_L\\ \Delta\hat{i}_{rL}\\ \Delta\hat{v}_{oL}\\ \Delta\hat{i}_{gL}\end{bmatrix} + B_{L2}\Delta\hat{v}_{bL} + B_{L1}V_o^{*}$$

$$\begin{bmatrix}\Delta\hat{i}_{oL}\end{bmatrix} = C_L\begin{bmatrix}\Delta\hat{\varphi}_L\\ \Delta\hat{\gamma}_L\\ \Delta\hat{i}_{rL}\\ \Delta\hat{v}_{oL}\\ \Delta\hat{i}_{gL}\end{bmatrix} \quad (13)$$

$$C_L = \begin{bmatrix}0 & 0 & 0 & \dfrac{1}{R_{LocalL}} & 1\end{bmatrix}$$

Note that the above model requires the PCC voltage at the leader unit. The PCC voltage can be easily estimated as,

$$\hat{v}_{bL} = v_{oFi} - i_{gFi}R_{LineFi}$$

$$\hat{v}_{bL} = C_e\begin{bmatrix}\Delta\varphi_{Fi}\\ \Delta\gamma_{Fi}\\ \Delta i_{rFi}\\ \Delta v_{oFi}\\ \Delta i_{gFi}\end{bmatrix} \quad C_e = [0 \quad 0 \quad 0 \quad 1 \quad -R_{LineFi}] \quad (14)$$

Combining the reference generation, local secondary controller, inner loop cascaded voltage and current controllers, LC filter and line dynamics, the full small-signal model of the follower system can be written as,

$$[\Delta\dot{x}_{Fi}] = A_{TFi}[\Delta x_{Fi}] + B_{TFi2}\Delta v_{bFi} + B_{TFi1}V_o^{*}$$

$$[\Delta x_{Fi}] = [\Delta\hat{\varphi}_L, \Delta\hat{\gamma}_L, \Delta\hat{i}_{rL}, \Delta\hat{v}_{oL}, \Delta\hat{i}_{gL}$$

$$\Delta\varepsilon_{Fi}, \Delta\varphi_{Fi}, \Delta\gamma_{Fi}, \Delta i_{rFi}, \Delta v_{oFi}, \Delta i_{gFi}]^T$$

$$A_{TFi} = \begin{bmatrix}A_L & 0_{5*1} & B_{L2}C_e\\ B_{s1}C_L & 0 & B_{s2}\\ B_{Fi1}D_{s1}C_L & B_{Fi1}C_s & A_{Fi} + B_{Fi1}D_{s2}\end{bmatrix} \quad (15)$$

$$B_{TFi2} = [0_{6*1} \quad B_{Fi2}]^T$$

$$B_{TFi1} = [B_{L1} \quad 0 \quad B_{Fi1}]^T$$

III. Sensitivity Analysis and Controller Design

A. Sensitivity Analysis

The follower system requires knowledge of the network parameters to build the virtual model of leader system and estimate the PCC voltage. The parameters of filters and local loads are often available. However, accurate line resistances are harder to obtain. The mismatch in the leader and follower line resistances can result in a current sharing error, as illustrated in Fig. 4. The results in Fig. 4 were obtained from multiple simulations with constant load. Initial parameters and network will be introduced in the next section. From Fig. 4 it is obvious that the sharing error is directly proportional to the mismatch in the line resistances.

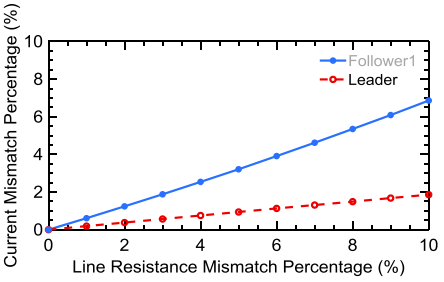

Fig. 4. Current sharing error percentage (error divided by leader current) with respect to line resistances mismatch.

B. Controller Design

Analysis of eigenvalues movement has been proven to be an efficient way to design the controller gains. Complete model of one follower system can be obtained by previously introduced modelling method. A large body of literature has already covered the selection of the inner loop PI gains and therefore they are not analyzed in this paper. Eigenvalues movements with respect to the increasing gains of the secondary layer PI controller are analyzed next to provide a brief guideline for designing the secondary control layer. The follower unit DG1 is analyzed. The eigenvalue analysis is done in MATLAB/SIMULINK. The parameters are listed in Table I.

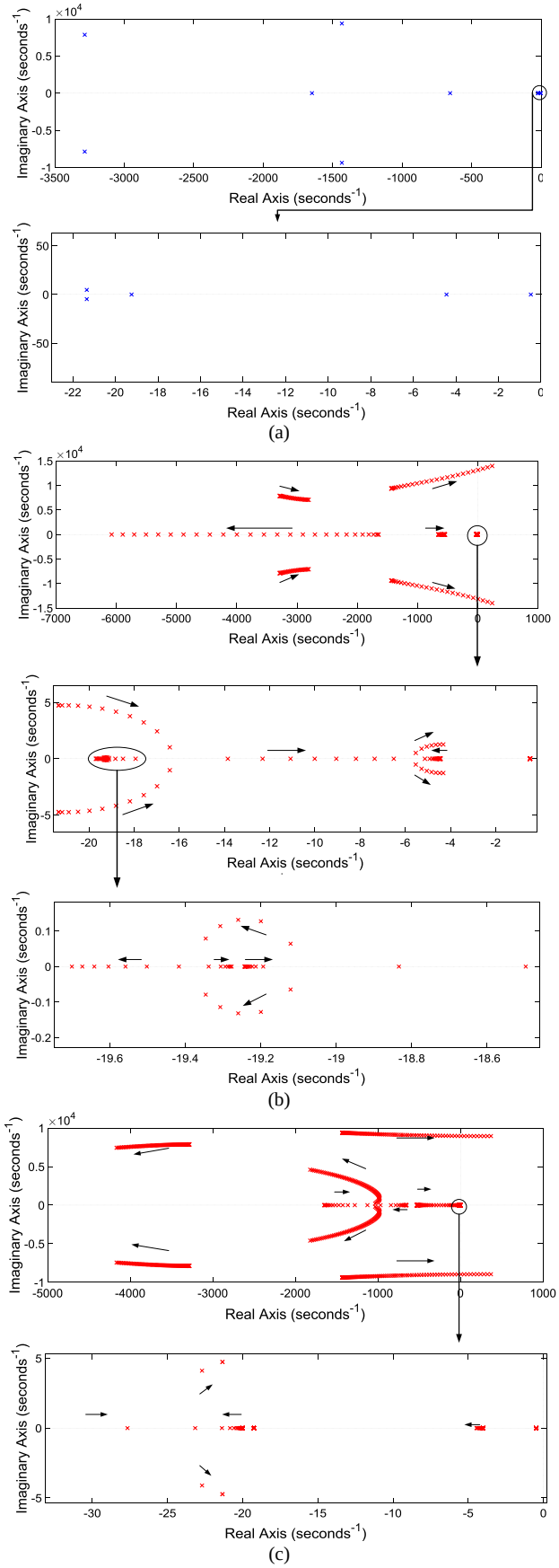

Fig. 5. Eigenvalue distribution: (a) Eigenvalues plot with initial parameters, (b) Eigenvalues movement with respect to K_{ps} increasing from 1 to 1.3. (c) Eigenvalues movement with respect to K_{is} increasing from 100 to 1000.

TABLE I: PARAMETERS

Parameter	Value	Parameter	Value
K_{pv}	0.5	R_{LineL}	0.3 Ω
K_{iv}	2	L_{LineL}	1.3 mH
K_{pc}	5	R_{LineF1}	0.5 Ω
K_{ic}	100	L_{LineF2}	1.1 mH
K_{ps}	1	R_{LineF2}	0.7 Ω
K_{is}	100	L_{LineF2}	1.5 mH
k_{F1}	1	R_{LocalL}	3 Ω
k_{F2}	1	$R_{LocalF1}$	6 Ω
R_f	0.01 Ω	$R_{LocalF2}$	9 Ω
L_f	1.8 mH	R_{Public}	5 Ω
C_f	45 μF	V_o^*	80 V

The eigenvalues plot with initial parameters is shown in Fig. 5 (a). As shown in the figure, all eigenvalues are in the left side domain, which suggest the system is stable. Fig. 5 (b) show the eigenvalues movement with respect to increasing K_{ps} ([1, 1.3]). According to the eigenvalues movement, increasing the K_{ps} significantly affects the system stability. The main trend is that the system becomes more and more oscillatory and finally unstable because multiple clusters of eigenvalues quickly move towards the imaginary axis. The stability limit for K_{ps} is around 1.15. From Fig. 5 (c), multiple clusters of eigenvalues move quickly towards negative infinity with increasing K_{is} ([100, 1000]), which suggest the stability is enhanced; however, there are still two clusters of eigenvalues moving towards positive domain, and thus a certain limitation for K_{is} exists. The stability limit for K_{is} is around 910. The follower system is clearly more sensitive to K_{ps} change. Thus, in general, it is better to keep a relatively small K_{ps} and then adjust K_{is} within the acceptable range to obtain a desired damping.

IV. SIMULATION RESULTS

Network model in Fig. 6 was built in MATLAB/SIMULINK. All parameters can be found in Table I. Initially, the load is 5 Ω and after 10s it is changed to 10 Ω. Two tests are performed: first, all units are chosen to share the load equally, second, the sharing ratio is changed to 4:2:1 (Leader unit DG0: Follower DG1: Follower DG2). The results are compared with the traditional droop control, with the droop coefficients set to 0.001 and 1.

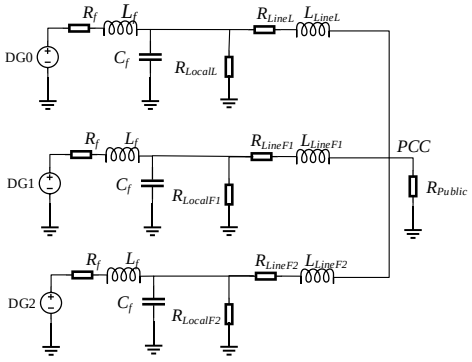

Fig. 6. Simulation network

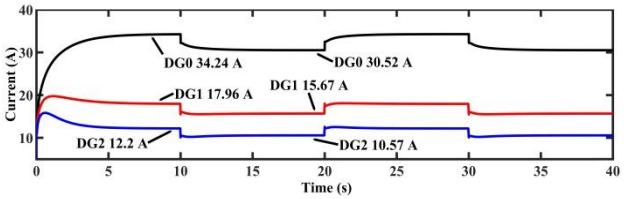

Fig. 7. Current sharing simulation results for traditional droop control (droop coefficient = 0.001).

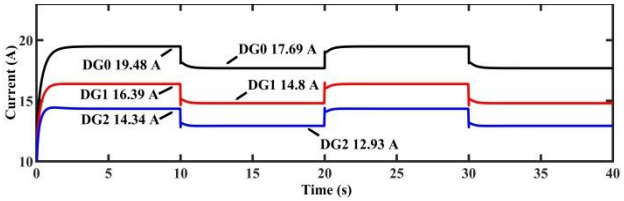

Fig. 8. Current sharing simulation results for traditional droop control (droop coefficient = 1).

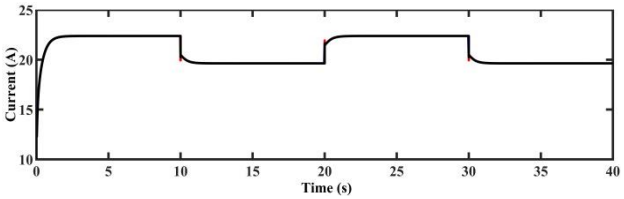

Fig. 9. Current sharing simulation results of proposed method.

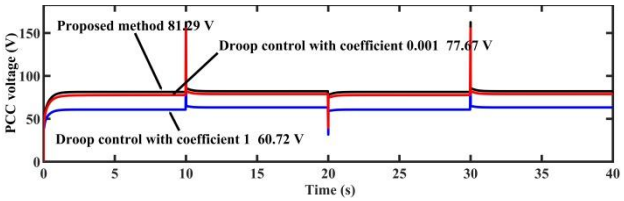

Fig. 10. Voltage regulation comparison at PCC.

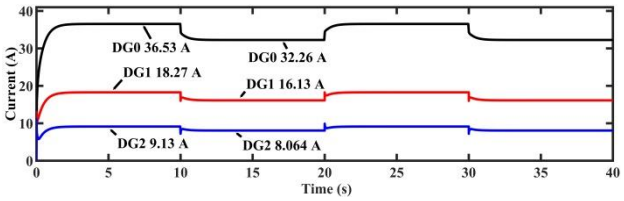

Fig. 11. Current sharing (DG0:DG1:DG2 = 4:2:1) simulation results of proposed method.

As shown in Fig. 7, the traditional droop control method has poor sharing accuracy with different line resistances and local loads. The sharing accuracy can be improved by choosing a larger droop coefficient, Fig. 8. However, such action results in worse voltage regulation. With the proposed method, all units can synchronize their current with high accuracy, Fig. 9. In Fig. 10, the voltage regulation results at the point of common coupling (the point where the public loads are connected) are compared. Results in Fig. 11 illustrate that the total current can be shared at the desired ratio (4:2:1) with high accuracy and the current sharing is maintained when the load changes.

V. Conclusion

This paper proposed a method which allows the DGs to share the currents at a desired ratio without using communication links. Compared to the traditional droop control, it suffers less from the line impedances effect, and has better voltage regulation at the PCC. The proposed method requires complete knowledge of the electrical network, and inaccurate parameter estimation can lead to a sharing error. The analysis of the sensitivity of the proposed system to inaccurate line parameters was presented. Eigenvalue analysis of the small-signal model of one follower system was performed to define acceptable controller gains. Finally, simulation in MATLAB/SIMULINK verified the performance of the proposed system.

Although the proposed method works well for single public load network, it cannot be directly applied to multiple public loads network. Future work should focus on extending the method to complex networks while the merits are maintained.

References

[1] B. Kroposki, R. Lasseter, T. Ise, S. Morozumi, S. Papathanassiou, and N. Hatziargyriou, "Making microgrids work," *IEEE Power and Energy Magazine*, vol. 6, no. 3, pp. 40-53, 2008.

[2] S. Morozumi, "Micro-grid demonstration projects in Japan," in *Proc. Power Conversion Conf.*, Nagoya, 2007, pp. 635-642.

[3] D. Salomonsson, L. Soder, and A. Sannino, "An adaptive control system for a DC microgrid for data centers," *IEEE Trans. on Industry Applications*, vol. 44, no. 6, pp. 1910-1917, 2008.

[4] A. Ipakchi and F. Albuyeh, "Grid of the future," *IEEE Power and Energy Magazine*, vol. 7, no. 2, pp. 52-62, 2009.

[5] N. Hatziargyriou, H. Asano, R. Iravani, and C. Marnay, "Microgrids," *IEEE Power and Energy Magazine*, vol. 5, no. 4, pp. 78-94, 2007.

[6] A. Kwasinski, "Quantitative evaluation of DC microgrids availability: Effects of system architecture and converter topology design choices," *IEEE Trans. on Power Electronics*, vol. 26, no. 3, pp. 835-851, 2011.

[7] Q. Shafiee, T. Dragičević, J. C. Vasquez, and J. M. Guerrero, "Hierarchical control for multiple DC-microgrids clusters," *IEEE Transa. on Energy Conversion*, vol. 29, no. 4, pp. 922-933, 2014.

[8] C. C. Chan, "An overview of electric vehicle technology," *Proc. of the IEEE*, vol. 81, no. 9, pp. 1202-1213, 1993.

[9] J. G. Ciezki and R. W. Ashton, "Selection and stability issues associated with a navy shipboard DC zonal electric distribution system," *IEEE Trans. on Power Delivery*, vol. 15, no. 2, pp. 665-669, Apr. 2000.

[10] S. P. Barave and B. H. Chowdhury, "Hybrid AC/DC power distribution solution for future space applications," in *Proc. IEEE Power Engineering Society General Meeting*, Tampa, FL, 2007, pp. 1-7.

[11] A. T. Ghareeb, A. A. Mohamed, and O. A. Mohammed, "DC microgrids and distribution systems: An overview," in *Proc. IEEE Power & Energy Society General Meeting*, Vancouver, BC, 2013, pp. 1-5.

[12] J. Robinson, D. Jovcic, and G. Joos, "Analysis and design of an offshore wind farm using a MV DC grid," *IEEE Trans. on Power Delivery*, vol. 25, no. 4, pp. 2164-2173, 2010.

[13] Operation and Integration of Distributed Resource Island Systems with Electric Power Systems, IEEE Standard 1547.42011, 2011, pp. 1–54.

[14] J. J. Justo, F. Mwasilu, J. Lee, and J. W. Jung, "AC-microgrids versus DC-microgrids with distributed energy resources: A review," *Renewable and Sustainable Energy Reviews*, vol. 24, pp. 387–405, Aug. 2013.

[15] S. Peyghami, H. Mokhtari, P. C. Loh, P. Davari, and F. Blaabjerg, "Distributed primary and secondary power sharing in a droop-controlled LVDC microgrid with merged AC and DC characteristics," *IEEE Trans. on Smart Grid*, vol. 9, no. 3, pp. 2284-2294, May 2018.

[16] N. Pogaku, M. Prodanovic, and T. C. Green, "Modeling, analysis and testing of autonomous operation of an inverter-based microgrid," *IEEE Trans. on Power Electronics*, vol. 22, no. 2, pp. 613-625, 2007.

[17] S. Anand and B. G. Fernandes, "Reduced-order model and stability analysis of low-voltage DC microgrid," *IEEE Trans. on Industrial Electronics*, vol. 60, no. 11, pp. 5040-5049, 2013.

[18] J. M. Guerrero, J. C. Vasquez, J. Matas, L. G. de Vicuna, and M. Castilla, "Hierarchical control of droop-controlled AC and DC microgrids—A general approach toward standardization," *IEEE Trans. on Industrial Electronics*, vol. 58, no. 1, pp. 158-172, 2011.

[19] P. C. Loh, D. Li, Y. K. Chai, and F. Blaabjerg, "Autonomous control of interlinking converter with energy storage in hybrid AC-DC microgrid," *IEEE Trans. on Industry Applications*, vol. 49, no. 3, pp. 1374-1382, 2013.

[20] S. Anand, B. G. Fernandes, and J. Guerrero, "Distributed control to ensure proportional load sharing and improve voltage regulation in low-voltage DC microgrids," *IEEE Trans. on Power Electronics*, vol. 28, no. 4, pp. 1900-1913, 2013.

[21] X. Lu, J. M. Guerrero, K. Sun, and J. C. Vasquez, "An improved droop control method for DC microgrids based on low bandwidth communication with DC bus voltage restoration and enhanced current sharing accuracy," *IEEE Trans. on Power Electronics*, vol. 29, no. 4, pp. 1800-1812, 2014.

[22] A. Bidram, F. L. Lewis, and A. Davoudi, "Distributed control systems for small-scale power networks: Using multiagent cooperative control theory," *IEEE Control Systems*, vol. 34, no. 6, pp. 56-77, 2014.

[23] M. Yazdanian and A. Mehrizi-Sani, "Distributed control techniques in microgrids," *IEEE Trans. on Smart Grid*, vol. 5, no. 6, pp. 2901-2909, 2014.

[24] A. Bidram, A. Davoudi, and F. L. Lewis, "A multiobjective distributed control framework for islanded AC microgrids," *IEEE Trans. on Industrial Informatics*, vol. 10, no. 3, pp. 1785-1798, 2014.

[25] Q. Shafiee, J. M. Guerrero, and J. C. Vasquez, "Distributed secondary control for islanded microgrids—A novel approach," *IEEE Trans. on Power Electronics*, vol. 29, no. 2, pp. 1018-1031, 2014.

[26] L. Meng, T. Dragicevic, J. Rold án-P érez, J. C. Vasquez, and J. M. Guerrero, "Modeling and sensitivity study of consensus algorithm-based distributed hierarchical control for DC microgrids," *IEEE Trans. on Smart Grid*, vol. 7, no. 3, pp. 1504-1515, 2016.

[27] Q. Li, F. Chen, M. Chen, J. M. Guerrero, and D. Abbott, "Agent-based decentralized control method for islanded microgrids," *IEEE Trans. on Smart Grid*, vol. 7, no. 2, pp. 637-649, 2016.

[28] S. Abhinav, I. D. Schizas, F. L. Lewis, and A. Davoudi, "Distributed noise-resilient networked synchrony of active distribution systems," *IEEE Trans. on Smart Grid*, vol. 9, no. 2, pp. 836-846, 2018.

[29] A. Pilloni, A. Pisano, and E. Usai, "Robust finite-time frequency and voltage restoration of inverter-based microgrids via sliding-mode cooperative control," *IEEE Trans. on Industrial Electronics*, vol. 65, no. 1, pp. 907-917, 2018.

Ruihao Song was born in Qingdao, China, in 1994. He received the B.Eng. degree in automation from Donghua University, Shanghai, in 2016. From 2016, he joined the University of New South Wales, Sydney, where he is currently pursuing the M.Phil degree in Electrical Engineering.

Branislav Hredzak (M'98–SM'13) received the B.Sc. and M.Sc. degrees from the Technical University of Kosice, Kosice, Slovak Republic, in 1993, and the Ph.D. degree from Napier University of Edinburgh, Edinburgh, U.K., in 1997, both in electrical engineering. He was a Lecturer and a Senior Researcher in Singapore from 1997 to 2007. He is currently a Senior Lecturer in the School of Electrical Engineering and Telecommunications, University of New South Wales, Australia. His current research interests include hybrid energy storage technologies and advanced control systems for power electronics and energy storage system.

B. T. Phung (M'87-SM'12) received a Ph.D. in Electrical Engineering from the University of New South Wales (UNSW Sydney), Australia in 1998. He is currently an Associate Professor in the School of Electrical Engineering and Telecommunications, UNSW. His research interests include dielectrics and electrical insulation materials, partial discharge, high-voltage phenomena and engineering applications, power system equipment design and condition monitoring methods, electromagnetic transients in power systems.